Materials Science & Engineering A 758 (2019) 86–95

Contents lists available at ScienceDirect

Materials Science & Engineering A

journal homepage: www.elsevier.com/locate/msea

High-temperature dependency of elastic mechanical behavior of two wrought magnesium alloys AZ31B and ZK60A studied by resonant ultrasound spectroscopy

E. Garlea[a,*], M. Radovic[c], P.K. Liaw[b]

[a] Development Department, CNS/Y-12 National Security Complex, Oak Ridge, TN, 37831, USA
[b] Department of Materials Science and Engineering, Texas A&M University, College Station, TX, 77843, USA
[c] Department of Materials Science and Engineering, University of Tennessee, Knoxville, TN, 37996, USA

ARTICLE INFO

Keywords:
Resonant ultrasound spectroscopy (RUS)
Tension test
Elastic mechanical behavior
High-temperature deformation
Internal friction
AZ31B and ZK60A magnesium alloys

ABSTRACT

Resonant ultrasound spectroscopy (RUS) was used to study the elastic mechanical properties and internal friction of two wrought magnesium alloys, AZ31B and ZK60A, from 25 °C to 450 °C. Samples in the rolled, transverse, and normal directions were characterized at 50 °C intervals to determine the temperature dependency of elastic moduli and stiffnesses for each direction. The temperature dependencies represented as, dE/dT, dG/dT, dB/dT, dC_{11}/dT, dC_{12}/dT, and dC_{44}/dT are provided herein. To evaluate the RUS technique for these type of alloys, Young's modulus was also determined by conventional static tension testing and the results were compared. From the same RUS experiment, the internal friction variation with temperature was calculated for both alloys. The linear coefficients of thermal expansion for each direction over the temperature range considered were determined, as they were needed to estimate sample dimension at elevated temperature for the RUS measurements.

This study shows that RUS can be a convenient and accurate technique to supply quantitative elastic mechanical data and fill the existing gaps on light metals characterization.

1. Introduction

Numerous experimental techniques, both static and dynamic, are available nowadays to determine elastic properties of engineering materials. Key static methods include tensile, compressive, flexural, and torsional tests. In general, direct measurements of stresses and strains are made during static methods, and the elastic moduli are determined from the slope of the linear region of the stress-strain curve. Dynamic methods, which include resonance and pulse means, provide advantages over static techniques because of the ease of specimen preparation, a wide variety of specimen shapes and sizes, great precision, and measurements over a wide temperature range. Radovic et al. [1] compared the experimental techniques of resonant ultrasound spectroscopy (RUS), impulse excitation, nanoindentation, and four-point bending by measuring the Young's and shear moduli. It was shown that dynamic methods (RUS and impulse excitation) have superior precision and repeatability, when compared to the static methods of nanoindentation and four-point bending.

When using static methods, measurements of elastic properties can become difficult at elevated temperatures. Khanna et al. [2] measured the Young's moduli from room temperature to 500 °C for two aluminum alloys using conventional tension testing and RUS. The Young's moduli measured employing both techniques were in agreement only at lower temperatures. At elevated temperatures, significant differences between the results were observed, which were attributed to the viscoplastic behavior of aluminum at high homologous temperatures and to the different strain rates between the two testing techniques.

The elastic mechanical properties are important to many design and engineering applications, as they are greatly dependent on temperature. These properties decrease rapidly with increasing temperature especially above 100 °C [3]. Mechanical vibration can cause significant damage in certain industrial applications. Therefore, the ability of a material to dissipate the elastic strain energy, known as the damping or internal friction, is important, since the damping capacity of a material can dissipate the undesirable noise and vibration as heat to the surroundings. Internal friction can be the result of a wide range of physical mechanisms, and it depends on the material microstructure, temperature, and frequency of the loading [4].

* Corresponding author. Y-12 National Security Complex, P.O. Box 2009 MS 8097, Oak Ridge, TN, 37831-8097, USA.
E-mail address: garleae@y12.doe.gov (E. Garlea).

https://doi.org/10.1016/j.msea.2019.04.115
Received 2 February 2019; Received in revised form 26 April 2019; Accepted 30 April 2019
Available online 03 May 2019
0921-5093/

Magnesium alloys are among the lightest metallic structural materials, but their strength diminishes at elevated temperature, which is reported to be due to activation of grain boundaries sliding (GBS) [5–10]. Recent studies on elasticity and internal friction also using RUS on ultrafine Mg-based alloys, including AZ31, showed that between 180 °C and 220 °C, the alloys underwent recrystallization and grain growth, a process that is completed around 300 °C [6]. The GBS mechanism decreases its activity with the grain growth process, since the number of grain boundaries are reduced.

As compared to their cast counterparts, wrought magnesium alloys exhibit improved mechanical properties, namely higher tensile strength, increased yield stress and fatigue resistance. Although alloying can improve the mechanical properties of pure polycrystalline magnesium, the damping properties are usually reduced with additions of alloying elements [11].

In this paper, the RUS technique was employed to evaluate two wrought magnesium alloys, AZ31B and ZK60A. The elastic mechanical properties of these alloys were studied experimentally from room temperature to 450 °C. Young's moduli were determined also using a conventional static technique (tension testing) to compare the two investigative techniques and to evaluate the potential advantages of RUS over conventional testing.

2. Experimental details

2.1. Materials and samples

Two wrought magnesium alloys, AZ31B and ZK60A, were used in this study. The nominal chemical compositions of those alloys are listed in Table 1.

Samples were prepared from the same plates as in Refs. [12–14] where the plate's history, microstructure, and starting texture are described in more detail. In short, the ZK60A commercial extruded plate, T5 temper, was partly solution-treated at 535 °C for 2 h, then quenched in hot water, and aged at 185 °C for 24 h. The AZ31B commercially rolled plate had a H24 temper, which involved strain hardening and partial annealing. For the ZK60A alloy the as-received microstructure was free of twinning with bimodal grain-size distribution consisting of larger (50–100 μm) and smaller grains (10–15 μm). Some twinning was identified in the microstructure of the AZ31B alloy and the average grain size was reported to be 15 μm. While the starting textures are typical of wrought magnesium alloys, there are some differences between the two alloys in the orientation of the c-axis of the hexagonal crystallographic structure. Specifically, ZK60A follows the typical combined rolled and extruded texture components, in which one major component has the basal poles perpendicular to the plate's normal direction, as seen in the schematic in Fig. 1. The second major component is with basal poles parallel to the transverse direction [12,15]. The as-rolled AZ31B alloy exhibits a radial symmetry, with the basal poles concentrated at the center, parallel to the normal direction, as the starting texture. The prismatic poles are randomly distributed in the rolling plane [16].

Test specimens were cut from the plate with their thickness (length) parallel to one of the major direction, the normal direction (ND), rolling or extruded direction (RD or ED), and transverse direction (TD), as visible in the schematic of Fig. 1. Fabrication of each sample was carried out using electro-discharge machining. Cylindrical samples were obtained for all three directions for the determination of coefficients of thermal expansion, and thin discs were obtained for dynamic elastic mechanical properties. For the static (conventional) Young's modulus measurements, tensile specimens in the ED/RD and TD were obtained. The plate's thickness did not allow machining of tensile specimens in the ND.

Table 1
Nominal chemical compositions for AZ31B and ZK60A (weight percent).

Material	Al	Zn	Zr	Mg	Temper
AZ31B	3.0%	1.0%	N/A	balance	H24
ZK60A	N/A	6.0%	0.5%	balance	T5

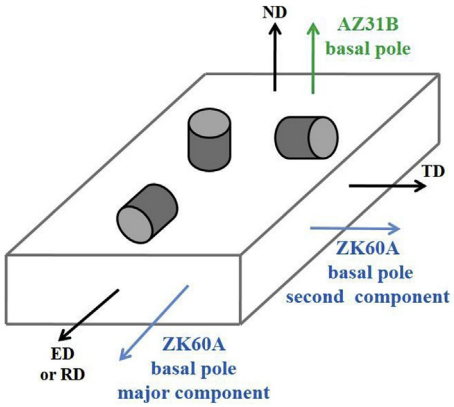

Fig. 1. Schematic showing the machine of cylinder and disc test specimens from the plate in the normal direction (ND), rolling or extruded direction (RD or ED), and transverse direction (TD). Tensile specimens were machined in RD and TD.

2.2. Coefficient of thermal expansion

A thermomechanical analyzer (Q400 EM, TA Instruments, DE) was used to measure the linear coefficient of thermal expansion (CTE). For both alloys, the CTE samples were machined from the as-received plates along the three different directions marked in Fig. 1. This approach allows for the linear CTE determination along each direction, revealing any thermally - anisotropic behavior due to texture effects. The samples were cylindrical in shape with a height and diameter of approximately 7.6 mm and 6.5 mm, respectively. During the thermomechanical measurements, nitrogen gas was flown in the specimen chamber at a rate of 100 mL/min. The experiment was carried out from room temperature (25 °C) to 450 °C using the expansion probe with a temperature ramp of 2 °C/min and an applied load of 1 N. Data collection was carried out at the rate of 0.5 s/point. For more details, the ASTM E831 standard describes the standard test method for the linear thermal expansion of solid materials by thermomechanical analysis [17].

2.3. Resonant ultrasound spectroscopy - determination of elastic moduli, stiffness, and internal friction

RUS is a unique and sophisticated nondestructive technique for determining the complete elastic tensor of a solid by measuring the resonant spectrum of mechanical resonance for a sample of known geometry, dimensions, and mass [18–21]. This technique permits the use of millimeter-sized samples, which in turn, presents a great advantage over the conventional testing in terms of material used and machining time required. RUS has successfully been used at temperatures as high as 1,500 °C [20] and as low as −270 °C [21]. For this study, the commercially available equipment for RUS (RUSpec, Magnaflux, IL) at room temperature was modified in-house for elevated temperatures for the determination of elastic moduli of materials at elevated temperatures [22]. A similar developed high-temperature RUS chamber has been proven as an accurate and practical system to determine elastic moduli of different metallic and ceramic materials in a 25 °C to 1,300 °C temperature range [1,2,23–26].

For the RUS experiments, thin disk samples were machined from the as-received plates with the height of the disc aligned in parallel to one of the three directions, as indicated in Fig. 1. At room temperature, each disc had the diameter of 24 mm and the thickness of 2 mm. In the case

of polycrystalline materials, the RUS technique is an average measurement over the all grains in the bulk, regardless of grain orientation or size. However, the texture affects the structural symmetry of the sample and the vibrational modes activated. In general, for a material with random grain orientation, the RUS data are analyzed using the isotropic mode. In this study, the take into consideration the texture effect, RUS data are analyzed by choosing the cubic mode to fit the data. The cubic mode has three independent elastic stiffnesses C_{11}, C_{12}, and C_{44} that are related to the three independent compliances S_{11}, S_{12}, and S_{44}, by the following equations [27]:

$$S_{11} = \frac{C_{11} + C_{12}}{(C_{11} - C_{12})(C_{11} + 2C_{12})} \quad (1)$$

$$S_{12} = \frac{-C_{12}}{(C_{11} - C_{12})(C_{11} + 2C_{12})} \quad (2)$$

$$S_{44} = \frac{1}{C_{44}} \quad (3)$$

The shear modulus is equal to $1/S_{44}$ and the Young's modulus can be calculated from compliance modulus, S_{ij} for each *hkl*. A multi-dimensional algorithm (RUSpec Quasar software, Quasar International, Albuquerque, NM) software was used to calculate the elastic constants assuming that macroscopic elastic constants are dominant by the grains with the preferred orientation. As such, the mechanical properties were not calculated for individual *hkls*. Moreover, using equation (4) [27,28], the anisotropy ratio was obtained for each preferred orientation to evaluate its effect on elasticity:

$$A = \frac{2C_{44}}{(C_{11} - C_{12})} \quad (4)$$

The RUS spectra cannot be deconvoluted directly to deduce the elastic constants. From the known sample dimensions, density, and a set of "guessed" elastic constants, an approximate spectrum is calculated. For both alloys in this study, the following initial "guessed" elastic constants were chosen: C_{11} = 57.7 GPa, C_{12} = 23.35 GPa, and $C44$ = 17.1 GPa [6]. These values are further refined once the measured frequencies are included into the software for calculations.

The RUSpec software minimizes the root-mean-square (RMS) error between the measured and calculated resonant peaks and enables the determination of the elastic constants from a single frequency scan. Measurements were taken for each sample in the 0 to 250 kHz frequency range, using the three - transducer setup. Goodness of fit was estimated using the RMS error between the measured and calculated frequency peaks. Overall, the first 40 resonant peaks were fitted for each sample with the exception of a few cases at elevated temperatures when it was challenging to clearly identify some peaks. Nevertheless, the goal of the measurement was to ensure the best goodness of fit possible. The experiments were carried out from room temperature, 25 °C, up to 450 °C, collecting data at 25 °C, 50 °C, and then every 50-degree interval to 450 °C. Before the RUS data were collected at elevated temperatures, the sample was held at a given temperature for 5 min to reduce temperature gradients. To avoid oxidation, the heating was executed in an argon environment.

In addition to the elastic moduli, the internal friction, Q^{-1}, was determined from the RUS spectra according to the following equation [18]:

$$Q_k^{-1} = \frac{\Delta\omega_k}{\omega_{k_0}} \quad (5)$$

where ω_{k_0} is the frequency associated with the kth eigenmode and $\Delta\omega_k$ is the full width at half maximum (FWHM) of that mode (FWHM of the frequency peak).

2.4. Conventional mechanical testing

Conventional static mechanical testing (CMT), namely tensile testing, was performed at 25 °C, 250 °C, and 450 °C. The room-temperature tension tests followed the procedures outlined in ASTM E8 [29], and the high-temperature tension tests were conducted, according to ASTM E21 [30]. The gage length and diameter of the tensile specimens were approximately 25.4 mm and 6.35 mm, respectively. For the AZ31B alloy, samples were machined with the gage length parallel to the RD and TD. In the case of the ZK60A alloy, samples were machined with the gage length parallel to the ED and TD, respectively. For each temperature, three tests were performed in each direction.

3. Experimental results and discussion

3.1. Young's modulus (E)

The Young's modulus (*E*) was determined by RUS and CMT to compare the results obtained from the two testing techniques.

For the RUS calculations, changes in the sample dimension need to be known as the temperature increases. This step was accomplished from the CTE studies carried out first. Fig. 2 (a) shows the dimensional change experimental data as a function of temperature for AZ31B with respect to the RD, TD, and ND. Each direction presents similar linear behavior from 25 °C up to 450 °C. The CTE, or α [μm/(m x °C)], is obtained by the linear fit of the experimental data using the following equation,

$$\alpha = \frac{\Delta L}{L_0 \Delta T} \quad (6)$$

where ΔL is the dimensional change (μm), L_0 is the original length of the specimen (mm or m × 10^{-3}), and ΔT is temperature range (°C) [17]. Table 2 is a summary of the CTE results for both alloys and the temperature ranges fitted linearly for calculation of CTE. The coefficient of determination, R^2, is included for each fitting. For AZ31B, the CTE

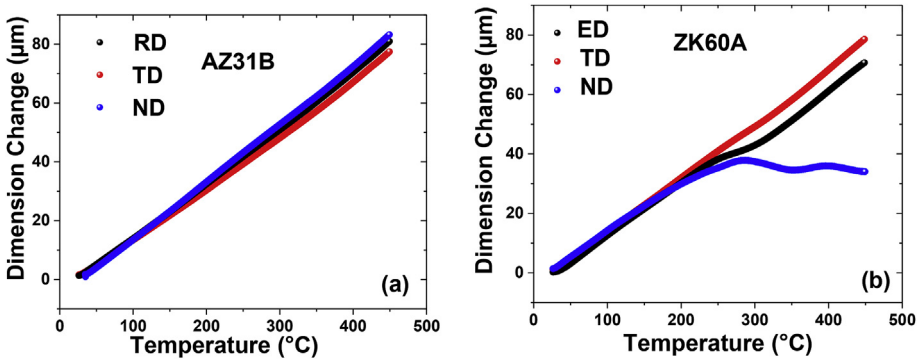

Fig. 2. Variation of the dimensional change with temperature from 25 °C to 450 °C for the a) AZ31B alloy and b) ZK60A used to calculate the linear coefficient of thermal expansion in RD, TD, and ND.

Table 2
Coefficient of thermal expansion (CTE) values for AZ31B and ZK60A calculated for specific temperature ranges, where R^2 is the coefficient of determination.

Material /Direction	CTE [μm/(m°C)]	Temperature range (°C)	R^2
AZ31B /RD	24.4	25–450	0.99956
AZ31B /TD	23.2	25–450	0.9990
AZ31B /ND	25.6	25-450	0.99985
ZK60A /ED	23.2	25–250	0.99943
ZK60A /ED	25.2	300–450	0.9988
ZK60A /TD	23.8	25–275	0.99978
ZK60A /TD	26.3	300–450	0.999
ZK60A /ND	19.2	25-285	0.98925

values were calculated to be 24.4 μm/(m°C), 23.2 μm/(m°C), and 25.6 μm/(m°C), in the RD, TD and ND, respectively. Fig. 2 (b) shows the thermal expansion experimental data as a function of temperature for the ZK60A alloy. Linear behavior is observed in the ED up to 250 °C with a CTE calculated to be 23.2 μm/(m°C). At this temperature, a gradual decrease in slope takes place, followed by an increase in slope with increasing temperature. Linear behavior is again observed with a CTE of 25.2 μm/(m°C) from 300 °C to 450 °C. In the TD, the sample undergoes a linear expansion up to 275 °C with a calculated linear CTE equal to 23.8 μm/(m°C). A slight change in slope is observed, followed by the linear behavior again with a CTE of 26.3 m/(m°C) from 300 °C to 450 °C. A more significant deviation from linearity is observed in the ND around 300 °C (282 °C) with a CTE of 19.2 μm/(m°C) over the linear interval. However, the same CTE value was used to calculate the sample dimension during the RUS study at and above 300 °C, since linearity in thermal expansion was not recovered above this temperature.

The quality of the linear fitting, represented by R^2, is close to 1 for all cases with the exception of ND for ZK60A. As such, with the exception of ND for ZK60A above 300 °C, it can be concluded that both alloys are reasonably isotropic in their linear thermal expansion behavior over the temperature interval considered.

Fig. 3 represents the first part of collected RUS spectra for ZK60A sample in ND from 25 °C and 350 °C. Spectra are plotted as amplitude, in arbitrary units, as a function of frequency, in kHz. Note that the resonance peaks shift toward lower frequencies, and they become broader as the testing temperature increases. The peak - shift is more significant at higher frequencies. The peak - shift is a result of the decrease of elastic constants with temperature, while the peak broadening is a result of an increase in internal friction (mechanical damping) with increasing temperature [18,20]. To process the RUS data, the CTE values determined for each sample were used to calculate the expected sample dimension at each temperature due to expansion during heating. Further, the Quasar software uses the calculated sample dimension to simulate the vibrational spectra. The mass of the sample at each temperature was assumed to be constant, whereas the density was recalculated for each temperature based on the expanded dimensions.

Table 3 is a summary of the elastic properties for both alloys for all

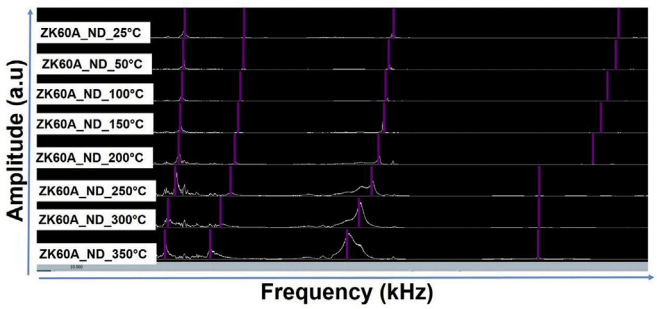

Fig. 3. First part of the RUS spectra obtained for ZK60A sample in the ND from 25 °C to 350 °C. Spectra are plotted as amplitude, in arbitrary units as a function of frequency, in kHz.

three directions at the temperatures measured. The table includes three independent stiffnesses, C_{11}, C_{12}, C_{44}, anisotropy factor (A), Young's modulus (E), shear modulus (G), bulk modulus (B), and Poisson's ratio (ν). The agreement between the location of measured frequencies and the predicted frequencies is observed in the value of RMS. Overall, there is a very good agreement with RMS being less than 1% for most of the cases. RMS greater than 1% were obtained in a few cases at 450 °C. Data from Table 3 are used for the graphs in Figs. 4, 7 and 8. As a general reference, the reported standard modulus properties at room temperature for magnesium and magnesium alloys are the following: $E = 45$ GPa, $G = 16.5$ GPa, and $\nu = 0.35$ [31]. However, these properties will be affected by processing history and chemical composition and indeed, they are somewhat different from our results in Table 3 at room temperature.

Fig. 4 shows variation of E with temperature for both alloys. An error bar is included for each data point, although they are hardly visible. The error bars were obtained by transforming the RMS error from % to GPa for each E value. All three directions follow a similar trend with E decreasing monotonically with increasing temperature. In the case of AZ31B, all three directions are in very close agreement for the entire temperature range. ZK60A exhibits E variation overall within the error bars. There is a slight separation of E_{ED} from the other two directions at 250 °C and 300 °C. For comparison, E determined from CMT, at temperatures of 25 °C, 250 °C, and 450 °C, are included in Fig. 4 for the RD and TD. The E determined by RUS in the ND direction is included in Fig. 4, although comparison values are not available from the CMT study. The CMT stress strain curves are shown in Figs. 5 and 6 at 25 °C, 250 °C, and 450 °C for AZ31B and ZK60A alloys. Three CMT tests were carried out for each temperature, and an averaged value is reported for each E in Fig. 4. The standard deviation is included as well. The CMT results show an almost perfect overlap between E_{ED} and E_{TD} for both alloys.

As visible in Fig. 4, at 25 °C the average values of E for AZ31B measured from CMT are lower than those measured using RUS, whereas the values of E for ZK60A measured from CMT are higher than those measured employing RUS. Despite the slight differences, the results from CMT and RUS at room temperature are considered to be in good agreement. At 250 °C, the average values of E for ZK60A measured from CMT are nearly the same as those determined by RUS, in both directions. The average values of E at 250 °C for AZ31B measured from CMT are slightly lower than those obtained using RUS at the same temperature. As the temperature increases to 450 °C, a significant difference is observed between the results obtained using CMT and RUS techniques. Both ZK60A and AZ31B alloys display at least a 10 to 15 GPa difference between the two techniques. The reasons for observed differences between the two techniques are multifold. First, RUS produces very small strains (on the order of 10^{-7}) and, consequently, very small stresses were exerted on the sample during testing when compared to the static mechanical testing. Additionally, deformation/strain rates in RUS are several orders of magnitude higher than those in static mechanical tests. Regardless of the differences in the magnitude of strains and strain rates between the two different methods, if the material studied behaves as a linear elastic solid, the differences in elastic moduli should be small, and this is the case here for both alloys up to 250 °C. However, at elevated temperatures, different mechanisms become active that result in an anelastic behavior. An anelastic behavior yields a larger impact in the elastic modulus from high strain rates, as in the case of CMT. One possible anelastic mechanism could be creep during static mechanical testing. The creep will result in a nonlinear relationship in the stress-strain curve, making the determination of the elastic moduli from CMT difficult, if not impossible. Most importantly, for Mg alloys, it is known that the GBS mechanism plays a major factor on the elastic properties [5–8]. The thermally activated GBS is a time dependent process as grain boundaries behave in a viscous manner, with the coefficient of viscosity depending exponentially on the temperature [4,32]. Therefore, for a given frequency of measurement, a

Table 3
Summary of the elastic properties determined using the RUS technique.

Temp. (°)	Material/Direction	C11 (GPa)	C12 (GPa)	C44 (GPa)	A	E (GPa)	G (GPa)	B (GPa)	ν	RMS (%)
25	AZ31B /RD	54.29	20.19	16.13	0.95	41.6	16.1	31.6	0.289	0.681
	AZ31B /TD	54.23	19.95	16.44	0.96	42.2	16.4	31.4	0.282	0.429
	AZ31B /ND	60.12	27.46	16.01	0.98	42.2	16	38.4	0.319	0.353
	ZK60A /ED	57.03	23.12	16.36	0.96	42.5	16.4	34.4	0.299	0.429
	ZK60A /TD	54.8	19.57	16.8	0.95	43	16.8	31.3	0.279	0.419
	ZK60A /ND	58.33	26.01	16.9	1.05	43.8	16.9	36.8	0.296	0.483
50	AZ31B /RD	53.9	20.26	15.97	0.95	41.2	16	31.5	0.289	0.658
	AZ31B /TD	53.98	20.17	16.14	0.95	41.5	16.1	31.4	0.287	0.394
	AZ31B /ND	58.73	26.59	15.53	0.97	41	15.5	37.3	0.32	0.433
	ZK60A /ED	56.28	22.77	16.13	0.96	41.9	16.1	34	0.299	0.383
	ZK60A /TD	53.29	18.8	16.47	0.96	42	16.5	30.3	0.276	0.583
	ZK60A /ND	58.02	26.24	16.75	1.05	43.5	16.8	36.8	0.297	0.512
100	AZ31B /RD	52.9	20.15	15.55	0.95	40.2	15.6	31.1	0.292	0.678
	AZ31B /TD	53.74	20.62	15.76	0.95	40.7	15.8	31.7	0.293	0.504
	AZ31B /ND	58.2	26.67	14.9	0.95	39.6	14.9	37.2	0.328	0.729
	ZK60A /ED	55.4	22.69	15.74	0.96	41	15.7	33.6	0.302	0.389
	ZK60A /TD	51.95	18.43	16.16	0.96	41	16.2	29.6	0.274	0.618
	ZK60A /ND	56.89	26.01	16.34	1.06	42.4	16.3	36.3	0.299	0.587
150	AZ31B /RD	51.97	19.94	15.17	0.95	39.3	15.2	30.6	0.294	0.693
	AZ31B /TD	51.91	19.54	15.45	0.95	39.8	15.5	30.3	0.288	0.546
	AZ31B /ND	57.25	26.38	14.51	0.94	38.6	14.5	36.7	0.33	0.548
	ZK60A /ED	54.41	22.52	15.35	0.96	40	15.4	33.2	0.304	0.385
	ZK60A /TD	51.67	18.68	15.55	0.94	40	15.6	29.7	0.285	0.529
	ZK60A /ND	56.04	25.78	15.9	1.05	41.4	15.9	35.9	0.302	0.506
200	AZ31B /RD	50.73	19.41	14.88	0.95	38.5	14.9	29.9	0.292	0.524
	AZ31B /TD	50.89	19.32	15.02	0.95	38.8	15	29.8	0.291	0.581
	AZ31B /ND	56.99	27.22	14.35	0.96	38.2	14.4	37.2	0.332	0.523
	ZK60A /ED	53.82	22.81	14.81	0.96	38.9	14.9	33.2	0.309	0.399
	ZK60A /TD	50.74	18.57	15.05	0.94	38.8	15.1	29.3	0.289	0.577
	ZK60A /ND	54.93	25.33	15.44	1.04	40.3	15.4	35.2	0.304	0.482
250	AZ31B /RD	48.7	18.21	14.46	0.95	37.3	14.5	28.4	0.289	0.463
	AZ31B /TD	49.96	19.33	14.59	0.95	37.8	14.6	29.5	0.294	0.597
	AZ31B /ND	55.95	26.87	13.8	0.95	36.9	13.8	36.6	0.336	0.786
	ZK60A /ED	51.84	20.01	13.71	0.86	36.2	13.7	30.6	0.320	0.491
	ZK60A /TD	49.02	18.12	15.03	0.97	38.5	15	28.4	0.279	0.674
	ZK60A /ND	54.67	26.55	14.8	1.05	38.9	14.8	35.9	0.314	0.878
300	AZ31B /RD	47.42	17.89	13.88	0.94	35.9	13.9	27.7	0.293	0.438
	AZ31B /TD	47.59	17.56	14.05	0.94	36.3	14.1	27.6	0.291	0.76
	AZ31B /ND	55.33	27.31	13.16	0.94	35.4	13.2	36.7	0.344	0.443
	ZK60A /ED	44.84	18.16	12.67	0.95	33	12.7	27.1	0.303	0.625
	ZK60A /TD	46.06	16.98	14.11	0.97	36.1	14.1	26.7	0.279	0.555
	ZK60A /ND	49.98	23.27	13.95	1.04	36.5	14	32.2	0.306	0.388
350	AZ31B /RD	46.79	18.25	13.37	0.94	34.8	13.4	27.8	0.3	0.925
	AZ31B /TD	46.74	18.09	13.79	0.96	35.6	13.8	27.6	0.291	0.858
	AZ31B /ND	54.22	27.19	12.41	0.92	33.6	12.4	36	0.352	0.789
	ZK60A /ED	47.84	21.98	12.47	0.96	33	12.5	30.6	0.324	0.671
	ZK60A /TD	44.55	18.44	12.47	0.96	32.6	12.5	27.2	0.306	0.79
	ZK60A /ND	49.92	25.47	12.66	1.04	33.7	12.7	33.7	0.33	0.417
400	AZ31B /RD	48.05	21.96	12.55	0.96	33.2	12.6	30.7	0.323	0.773
	AZ31B /TD	46.94	19.6	12.67	0.93	33.3	12.7	28.7	0.315	0.965
	AZ31B /ND	54.01	28.44	11.77	0.92	32.0	11.8	37	0.361	0.799
	ZK60A /ED	49.62	25.09	10.78	0.88	29.4	10.8	33.3	0.322	0.726
	ZK60A /TD	43.32	17.83	12.08	0.95	31.6	12.1	26.3	0.307	0.873
	ZK60A /ND	53.02	30.25	11.49	1.01	31.3	11.5	37.8	0.362	0.441
450	AZ31B /RD	44.6	19.66	11.89	0.95	31.4	11.9	28	0.318	0.976
	AZ31B /TD	44.22	19.39	12.15	0.98	31.9	12.2	27.7	0.311	1.698
	AZ31B /ND	51.36	27.15	11.42	0.94	31	11.4	35.2	0.357	1.058
	ZK60A /ED	39.86	16.96	10.47	0.91	27.7	10.5	24.6	0.322	0.726
	ZK60A /TD	38.52	12.26	12.26	0.93	31.4	12.4	21.0	0.262	0.997
	ZK60A /ND	44.47	23.41	11.02	1.05	29.4	11	30.4	0.335	0.611

temperature can be reached at which the viscosity will be low enough to activate GBS. This phenomenon can take place even at reasonably small stresses. The motion of the grain boundaries relaxes the shear stress acting on the grain boundaries, and a lower apparent value of the Young's modulus will be measured. The temperature at which the viscous flow at grain boundaries occurs depends on the test method and increases with the rise in frequencies. In fact, evidence suggests that GBS occurs in magnesium alloys at temperatures as low as 200 °C [9,33,34]. Thus, the expected temperature at which the viscous flow will become significant would be much higher for the dynamic method (RUS) than for the static method (CMT).

Furthermore, at 250 °C the average values of *E* for ZK60A measured from CMT are near the same as those measured using RUS, whereas the average values of *E* for AZ31B at 250 °C measured from CMTs were somewhat lower than those using RUS. This is believed to be an effect induced by differences in grain size between the two alloys as it was reported that the onset temperature of GBS can increase with increasing grain size [5,10]. The ZK60A alloy has a mixed grain size microstructure, with the larger grains approaching 100 μm, while AZ31B has smaller grains near 15 μm. Thus, the smaller grains in the AZ31B alloy could permit activation of GBS at a lower temperature when compared to the ZK60A alloy. This is in agreement with the damping properties

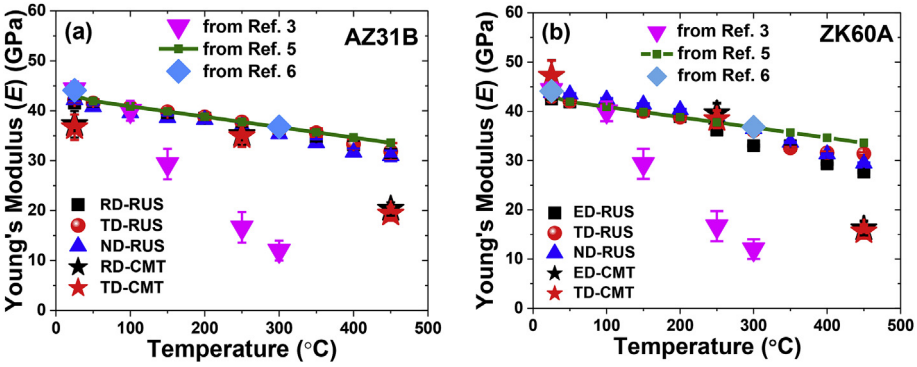

Fig. 4. Comparison of the average values for E obtained from CMT and RUS for the a) AZ31B alloy and b) ZK60A alloy. Literature values are inserted.

that will be discussed in Section 3.3.

Finally, the RUS results are compared to those reported by Ref. [5] (green symbol-line in Fig. 4) and Ref. [6] (symbol) which also used ultrasonic based testing techniques and have clear microstructural similarities and differences in the testing material. At room temperature, there is reasonable good agreement between reported E and our results for both alloys. In the case of AZ31B, literature values are somewhat more elevated. In particular, E = 43.0 GPa at room temperature was reported for a hot rolled sheet [5] which had similar texture and average grain size with our material. Larger grain size was reported for hot rolled plate case, which also had basal texture, but a slightly different E = 43.8 GPa [5]. In the case of AZ31 in Ref. [6], the alloy was treated through four equal channel angular pressing passes, resulting in a slightly larger E, as visible in Fig. 4 (a). Both references [5,6] assumed isotropic behavior for the calculation of elastic properties. For the effect of temperature on elastic moduli, the green symbol-line in Fig. 4 was obtained using dE/dT of −0.0209 from room temperature to 450 °C and E = 43.0 GPa [5]. It is noted that the slope value of −0.0209 was reported for the solution treated material, which had random starting grain orientation and significantly larger grain size [5]. This case follows a linear decrease in E with increasing temperature very similar to our results for AZ31B up to 450 °C and with AZ60A up to 250 °C. On the other hand, the hot rolled sheet is reported to deviate from linearity around 200 °C [5]. A somewhat similar trend was reported for the hot rolled plate material but data is not available above 300 °C [5] and these trends are in better agreement with ZK60A. When comparing our results to the material processed through the equal channel angular pressing, it is observed an excellent agreement at 300 °C for AZ31B. It can be concluded that when similar ultrasonic testing techniques are employed, texture and grain size are not significantly affecting the Young's modulus. In the case of conventional testing, Quan [3] reports on AZ31B values for Young's modulus that were obtained by CMT on samples deformed in TD. Although from room temperature to 100 °C results are in agreement with RUS, E values are significantly lower than this study at 250 °C and 300 °C.

3.2. Elastic constant variation with temperature determined using RUS

The temperature dependency of E in RD for AZ31B and ED for ZK60A, and the corresponding stiffnesses C_{11}, C_{12}, and C_{44} in RD, are shown in Fig. 7 (a) and (b), respectively. Overall, for both alloys, these elastic constants decrease with increasing temperature and are very similar from room temperature to approximately 250 °C. ZK60A shows significant fluctuation in E_{ED} above 250 °C whereas E_{RD} for AZ31B maintains a linear behavior over the entire temperature range, Fig. 7 (a). The room temperature stiffness results for ZK60A agree very well with those reported by Ref. [6] for AZ31 alloy as seen in Fig. 7 (b).

The anisotropy ratio, A, was calculated with equation (4) and shown in Table 3 for each direction, for both alloys, and for all temperatures studied. When A = 1 the material is isotropic and deviation from unity indicates anisotropic behavior [28]. In Table 3, it is visible that for all cases A is different than 1. This suggests that these two alloys are not fully isotropic at room temperature nor at elevated temperatures. However, the slight deviation from 1, with an average of A = 0.96 ± 0.04 indicates that there is not significant elastic anisotropy among the three directions, even though the starting materials were textured. Therefore, the temperature range of 25 °C–450 °C has no significant effect on anisotropy for these two alloys when tested in the elastic regime.

To quantify the temperature dependency of elasticity, linear fitting was performed for each constant over the temperature range that exhibited a linear trend. The slopes, represented by dE/dT, dC_{11}/dT, dC_{12}/dT and dC_{44}/dT are presented in Table 4. The R^2 values suggest overall good fitting with the exception of the slope for C_{12} for the ZK60A alloy. The C_{44} for both alloys undergoes little slope change with increasing temperature. A similar trend is observed for C_{12} for AZ31B up to 300 °C and ZK60A up to 200 °C. Consistent results were reported for C_{12} for ultrafine grain AZ31 alloy [6]. In can be concluded that there is a linear dependency of elastic constants with temperature from room temperature to 250 °C and that the variation of elasticity with temperature for both alloys follows similar trends.

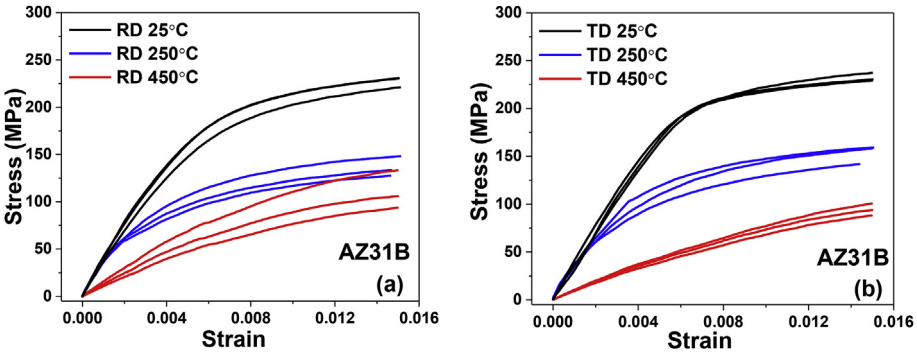

Fig. 5. Stress-strain curves obtained at 25 °C, 250 °C, and 450 °C from CMT for the AZ31B alloy in (a) RD and (b) TD.

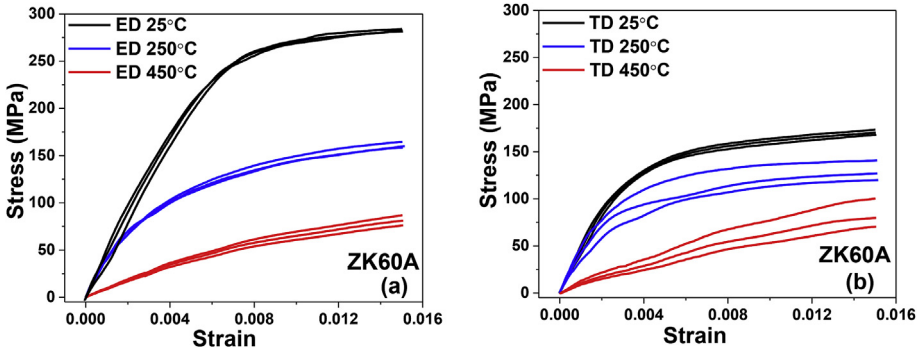

Fig. 6. Stress-strain curves obtained at 25 °C, 250 °C, and 450 °C from CMT for the ZK60A alloy in (a) ED and (b) TD.

The graphs in Fig. 8(a–c) represent the variation with temperature for G, B, and ν for AZ31B and Fig. 8(d–f) for ZK60A. The error bar is obtained again for each data point by calculating the RMS % from the specific property value. AZ31B exhibits a monotonic decrease in G with increasing temperature and the three directions agree within the error bar. ZK60A has G decreasing linearly with increasing temperature from 25 °C to 200 °C and there is good agreement among the three directions. At 250 °C, G_{ED} separates from the other two directions maintaining the most linear trend overall. When G is compared with literature values, the agreement is not as good as that observed for E. A value of $G = 15.5$ GPa at room temperature was reported by Ref. [5] for the hot rolled sheet and $G = 15.8$ GPa for the hot rolled plate.

The slope of -0.012 reported for the solution treated material and $G = 15.5$ GPa for room temperature [5] were used to calculate the line in Fig. 8 (a) and (b). There is no agreement with our results. The dG/dT slope of -0.0088 reported for pure Mg [35] and $G = 15.5$ GPa for the room temperature value [5] were used to calculate the symbol-line curve and somewhat agrees with AZ31B over the entire temperature range. ZK60A results start to overlap with the symbol-line curve at approximately 250 °C for G_{ED}. In general, the literature values from both sources are smaller than our results.

In the case of B and ν, Fig. 8 (b-c, e-f), both alloys exhibit similar behavior with some specific differences. Fig. 8 (b) and (c) for AZ31B, the ND deviates significantly from RD and TD, which in turn, are very similar. However, all three directions follow the same trends in B and ν with increasing temperature. B_{ND} has almost negligible change in slope for the entire temperature range, as seen in Table 5. Table 5 is a summary of temperature dependency for E on TD and ND and G and B on all three directions. The temperature range used for the linear fitting is included along with the coefficient of determination. The room temperature value is included as well. Further, a deviation from the monotonic decrease with increasing temperature is observed around 300 °C for B_{RD} and B_{TD} for AZ31B alloy. B increases at 400 °C than decrease at 450 °C. A similar but more accentuated pattern is undergone by ZK60A, with B_{ED} and B_{ND} significantly increasing at 350 °C and 450 °C then decreasing at 450 °C. For ZK60A, B_{ED}, B_{TD}, and B_{ND} have different magnitudes and B_{TD} has a linear behavior up to 400 °C. A comparison value is included in the graphs, obtained for ZK31 [6], which agrees with B_{ED} results for ZK60A. Poisson's ratio increases with increasing temperature for all data sets. The ν_{ND} for AZ31B and ν_{TD} for ZK60A separate from the other two directions. A linear behavior is exhibited by ZK31B up to 350 °C when an abrupt jump takes place. ZK60A shows more variation in ν below 300 °C than ZK31B and even a more significant jump in results at 350–400 °C.

The elastic mechanical properties studied here show consistently linear behavior from room temperature to approximately 250 °C. E and G are similar for all three directions whereas B and ν for ND, in the case of ZK31B, and for TD, in the case of ZK60A, separate from the other two directions. The distinct separation for the properties along these two directions is believed to be due to the characteristics of the starting texture. ZK31B has the (0001) family of grains orientated parallel to ND and the second basal pole component is parallel to TD for ZK60A. Texture evolution during heating was not observed to occur at temperature below 250 °C but changes in basal poles were reported at 350 °C for an AZ31B alloy with a similar starting texture [36]. Recrystallization and grain growth have been reported at temperature greater than 300 °C [6,31] that can affect texture and subsequently explain the significant jump in B and ν in the 300–400 °C range.

3.3. Internal friction

The temperature dependency of the internal friction on RD for AZ31 and ZK60 are shown in Fig. 9. The frequencies of the peaks at room temperature used in this study were 25.26 kHz and 27.40 kHz for ZK60A and AZ31B, respectively. The same peaks were monitored for all temperatures studied, although their position shifted as expected with temperature. From 25 °C up to approximately 200 °C, ZK60A and AZ31B alloys display similar behavior with damping capacities slightly

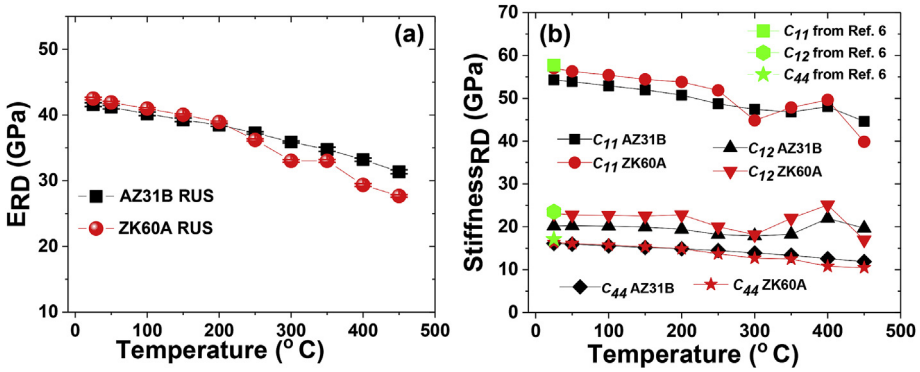

Fig. 7. Variation of elastic constants on the RD with temperature: (a) E and (b) the stiffnesses C_{11}, C_{12}, and C_{44} for AZ31B and ZK60A alloys. C_{11}, C_{12}, and C_{44} reported by Ref. [6] are for AZ31 alloy.

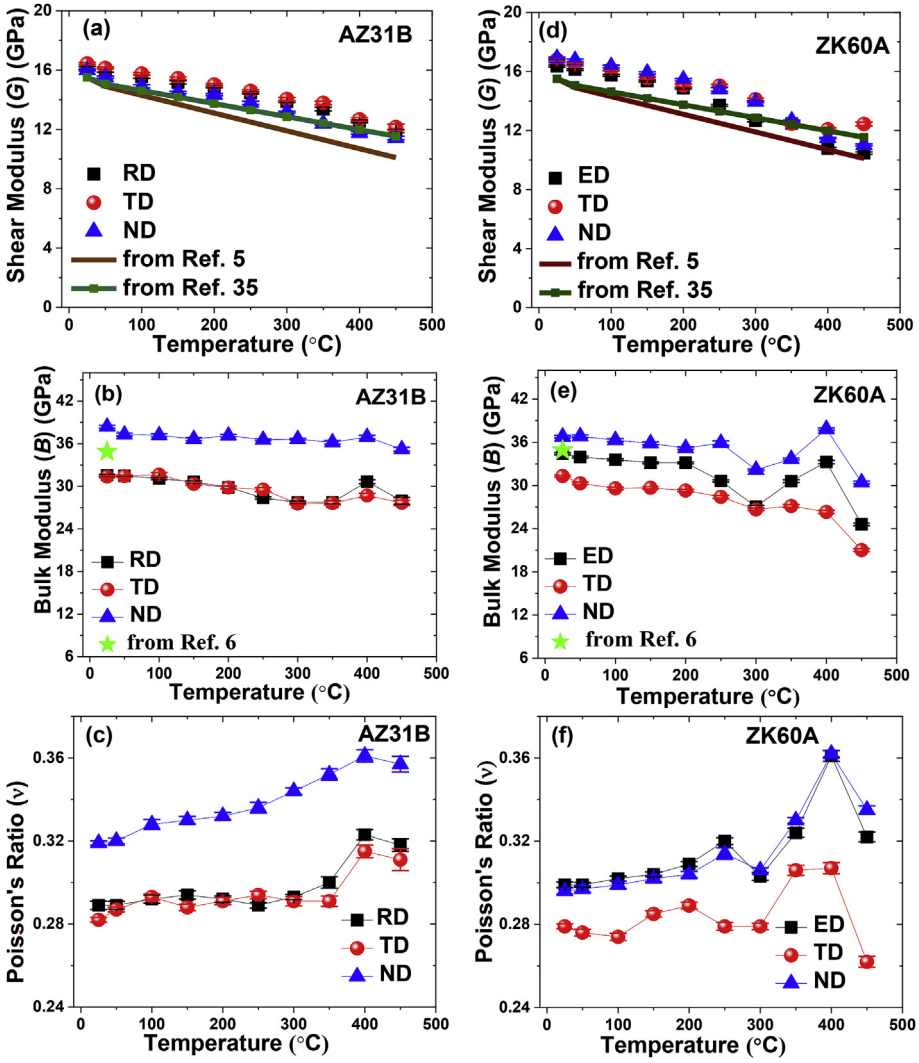

Fig. 8. Elastic moduli: G, B, and ν variation with temperature for (a–c) AZ31B and (d–f) ZK60A. All three directions are shown.

Table 4
Summary of dE/dT, dC_{11}/dT, dC_{12}/dT, and dC_{44}/dT for AZ31B and ZK60A on RD.

Material	Property	Slope (GPa/°C)	R^2	Property at 25 °C (GPa)	Temperature range for slope calculation (°C)
AZ31	E	-0.02302	0.97987	41.6	25-450
	C_{11}	-0.02461	0.98331	54.3	25-350
	C_{12}	-0.00797	0.83988	20.2	25-350
	C_{44}	-0.00966	0.9747	16.1	25-450
ZK60	E	-0.03529	0.957	42.5	25-450
	C_{11}	-0.0211	0.966	57.0	25-250
	C_{12}	-0.01553	0.6517	23.1	25-300
	C_{44}	-0.01451	0.96423	16.4	25-450

Table 5
Summary of dE/dT on TD and ND; dG/dT and dB/dT for AZ31B and ZK60A on RD, TD and ND.

Material	Property	Slope (GPa/°C)	R^2	Property at 25 °C (GPa)	Temperature range for slope calculation (°C)
AZ31	E_{TD}	-0.02151	0.98417	42.17	25-450
	E_{ND}	-0.02506	0.97881	42.22	25-450
	G_{RD}	-0.00954	0.96557	16.13	25-450
	G_{TD}	-0.009	0.97676	16.44	25-450
	G_{ND}	-0.0105	0.98626	16.01	25-450
	B_{RD}	-0.01331	0.93997	31.56	25-350
	B_{TD}	-0.01297	0.90169	31.37	25-350
	B_{ND}	-0.00424	0.57882	38.35	50-450
ZK60	E_{TD}	-0.02849	0.95649	42.97	25-450
	E_{ND}	-0.0353	0.96484	43.79	25-450
	G_{ED}	-0.01442	0.95957	16.36	25-450
	G_{TD}	-0.01147	0.93884	16.80	25-450
	G_{ND}	-0.01489	0.9563	16.89	25-450
	B_{ED}	-0.02044	0.68092	34.42	25-300
	B_{TD}	-0.01331	0.91696	31.31	25-400
	B_{ND}	-0.01669	0.81844	36.78	25-300

increasing with temperature. However, above 200 °C for AZ31B and above 300 °C for ZK60A, the damping capacity of both alloys increases significantly with temperature.

Fig. 9 is another evidence of the anelastic relaxation due to GBS above 200 °C. Internal friction is generally defined as the dissipation of the elastic-mechanical energy in the material [11]. If GBS is activated as a dissipation mechanism at a certain temperature, the damping capacity increases with temperature because the sliding of the grain boundaries converts the mechanical energy into thermal energy as a result of internal friction at grain boundaries. The slope change for AZ31B at 200 °C is the onset temperature of internal friction parameter. A temperature of 180 °C was the onset of internal friction for ultrafine AZ31 alloy [6]. Grain size affects greatly the damping capability and GBS.

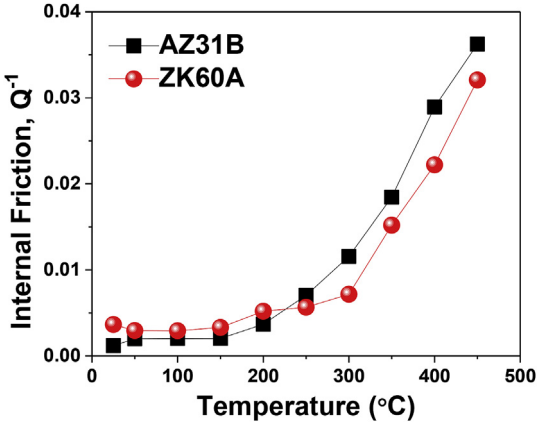

Fig. 9. Temperature dependence of internal friction in AZ31B and ZK60A in RD.

Larger grain size will reduce the onset temperature of GBS mechanisms and will decrease its magnitude [5,6,10]. In the presence of large grains, the GBS activity decreases because of reduced number of grain boundaries. ZK60A, which has grains larger than ZK31B, has the onset of internal friction delayed by approximately 100 °C, which is the change in slope at 300 °C. At 300 °C, for example, ZK60A has inferior damping capacity than ZK31B, pattern that is maintained to 450 °C.

The sharp increase in the damping capacity above 200 °C coincides with the changes in slope and deviations from linearity of the elastic mechanical constants. The observed changes in the elastic mechanical propertied and damping capacity are due to the same mechanism, namely the GBS. While the GBS is activated in the case of both testing techniques, RUS and CMT, the RUS technique allows the measurement of true elasticity, providing quantitative elastic properties. The GBS phenomenon is believed to be more pronounced in the case of conventional mechanical testing.

4. Conclusions

The elastic mechanical properties of two wrought magnesium alloys, AZ31B and ZK60A, were studied from room temperature to 450 °C using dynamic mechanical testing. Measurements were conducted using a Resonant Ultrasound Spectroscopy instrument and small cylindrical specimens prepared in RD, TD, and ND. Elastic moduli, *E, G, B,* and the Poisson's ratio were determined at several temperatures allowing the calculation of the temperature dependency, as dE/dT, dG/dT, and dB/dT in all three directions. These results are provided here for both alloys. In addition, the temperature dependency of stiffnesses, dC_{11}/dT, dC_{12}/dT, and dC_{44}/dT in RD were calculated and reported.

Using conventional static tensile testing and dog bone specimens the Young's modulus was determined at 25 °C, 250 °C, and 450 °C and the results from the two techniques were compared. At lower temperatures (at or below 250 °C), the Young's moduli obtained from static testing agreed well with the RUS results. However, at higher temperatures (above 250 °C), the apparent Young's moduli from conventional testing were significantly lower. The observed differences were attributed to the effect of anelastic mechanisms, such as grain boundary sliding as the main mechanism and creep. This phenomenon is enhanced by the combination of high strain rates in the case of static deformation and elevated temperature. In addition, the small grain size in ZK31B, yields even a lower onset temperature for the grain boundary sliding, which is around 200 °C in this case. The sharp increase in the damping capacity of the two alloys occurs near 200 °C and it is consistent with the slope change and deviations from linearity of the elastic constants.

Finally, as part of the elastic modulus determination at elevated temperature, a study was conducted for determination of the linear coefficient of thermal expansion in all three directions.

While providing a wealth of quantitative experimental data for these two Mg alloys that can be further used for modeling, it has been proven here that when only the elastic mechanical properties are needed, RUS can be superior approach than conventional testing. In one experiment, the elastic moduli and stiffnesses can be determined allowing the true elasticity to be differentiated from inelastic strains. In addition, sample preparation involves less material, less machining, and can accept smaller sample size, thus samples in the normal direction could be machined from the plate in this case.

Acknowledgement

Funding for this research was provided by the CNS/Y-12 National Security Complex under the Plant Directed Research, Development, and Demonstration program. NSF grant to Texas A&M University (award # 1726887) is also acknowledged for support.

Authors acknowledge Dr. M. W. Freels for his contribution to the project while working at the University of TN/Y-12 National Security Complex.

Appendix A. Supplementary data

Supplementary data to this article can be found online at https://doi.org/10.1016/j.msea.2019.04.115.

5. Disclaimer and copyright notice

References

[1] M. Radovic, E. Lara-Curzio, L. Riester, Comparison of different experimental techniques for determination of elastic properties of solids, Mater. Sci. Eng. 368 (2004) 56–70.
[2] S.K. Khanna, X. Long, W.D. Porter, H. Wang, C.K. Liu, M. Radovic, E. Lara-Curzio, Determination of thermophysical and thermomechanical properties of 5754 and 6111 aluminum alloys for spot welding simulation application, Sci. Technol. Weld. Join. 10 (1) (2005) 82–87.
[3] G. Quan, Yield and plastic deformation of Mg-alloy AZ31 at elevated temperatures, Mater. Sci. Forum 488–489 (2005) 623–628.
[4] G. Gremaud, S. Kustov, O. Bremnes, Mechanical spectroscopy, with applications to materials science, Mater. Sci. Forum 366–368 (2001).

[5] H. Watanabe, T. Mukai, M. Sugioka, K, Ishikawa, Elastic and damping properties from room temperature to 673 K in an AZ31 magnesium alloy, Scripta Mater. 51 (4) (2004) 291–295.
[6] M. Janovská, P. Minárik, P. Sedlák, H. Seiner, M. Knapek, F. Chmelík, M. Janeček, M. Landa, Elasticity and internal friction of magnesium alloys at room and elevated temperatures, J. Mater. Sci. 53 (11) (2018) 8545–8553.
[7] T. Ke, Experimental evidence of the viscous behavior of grain boundaries in metals, Phys. Rev. 71 (1947) 533–546.
[8] C. Zener, Theory of the elasticity of polycrystals with viscous grain boundaries, Phys. Rev. 60 (1941) 906–908.
[9] J. Koike, R. Ohyama, T. Kobayashi, M. Suzuki, K. Maruyama, Grain-boundary sliding in AZ31 magnesium alloys at room temperature to 523 K, Mater. Trans. 44 (4) (2003) 445–451.
[10] R.N. Stevens, Grain-boundary sliding in metals, Metall. Rev. 11 (1966) 129–142.
[11] X.S. Hu, Y.K. Zhang, M.Y. Zheng, K. Wu, A study of damping capacities in pure Mg and Mg–Ni alloys, Scripta Mater. 52 (11) (2005) 1141–1145.
[12] L. Wu, A. Jain, D.W. Brown, G.M. Stoica, S.R. Agnew, B. Clausen, D.E. Fielden, P.K. Liaw, Twinning–detwinning behavior during the strain-controlled low-cycle fatigue testing of a wrought magnesium alloy, ZK60A, Acta Mater. 56 (2008) 688–695.
[13] L. Wu, G.M. Stoica, H.H. Liao, S.R. Agnew, E.A. Payzant, G. Wang, D.E. Fielden, L. Chen, P.K. Liaw, Fatigue-property enhancement of magnesium alloy AZ31B through equal-channel-angular pressing, Metall. Mater. Trans. 38A (2007) 2283–2289.
[14] L. Wu, Mechanical Behavior and the Role of Deformation Twinning in Wrought Magnesium Alloys Investigated Using Neutron and Synchrotron X-Ray Diffraction, Ph.D. thesis University of Tennessee, Knoxviile, 2009.
[15] L. Wu, S.R. Agnew, D.W. Brown, G.M. Stoica, B. Clausen, A. Jain, D.E. Fielden, P.K. Liaw, Internal stress relaxation and load redistribution during the twinning-detwinning-dominated cyclic deforamtion of a wrought magnesium alloy, ZK 60A, Acta Mater. 56 (2008) 3699–3707.
[16] L. Wu, S.R. Agnew, Y. Ren, D.W. Brown, B. Clausen, G.M. Stoica, H.R. Wenk, P.K. Liaw, The effects of texture and extesnion twinning on the low-cycle fatigue behavior of a rolled magnesium alloy, AZ31B, Mater. Sci. Eng. 527 (2010) 7057–7067.
[17] ASTM, "ASTM E831, Standard Test Method for Linear Thermal Expansion of Solid Materials by Thermomechanical Analysis," ASTM International..
[18] A. Migliori, J.L. Sarrao, Resonant Ultrasound Spectroscopy: Applications to Physics, Materials Measurements, and Nondestructive Evaluation, John Wiley, New York, NY, 1997.
[19] O.L. Anderson, D. Isaak, H. Oda, High-temperature elastic constant data on minerals relevant to geophysics, Rev. Geophys. 30 (1) (1992) 57–90.
[20] R.G. Leisure, F.A. Willis, Resonant ultrasound spectroscopy, J. Phys. Condens. Matter 9 (28) (1997) 6001–6029.
[21] Z. Zhang, V. Keppens, P.K. Liaw, Y. Yokoyama, A. Inoue, Elastic properties of Zr-based bulk metallic glasses studied by resonant ultrasound spectroscopy, J. Mater. Res. 22 (2) (2007) 364–367.
[22] M.A. Steiner, E. Garlea, J. Creasy, A. DeMint, S.R. Agnew, Temperature dependent elastic properties of γ-phase U–8 wt% Mo, J. Nucl. Mater. 500 (2018).
[23] M. Radovic, M.W. Barsoum, A. Ganguly, T. Zhen, P. Finkel, S.R. Kalidindi, E. Lara-Curzio, On the elastic properties and mechanical damping of Ti3SiC2, Ti3GeC2, Ti3Si0.5Al0.5C2 and Ti2AlC, in the 300-1573 K temperature range, Acta Mater. 54 (2006) 2757–2767.
[24] S. Kota, M. Agne, E. Zapata-Solvas, O. Dezellus, D. Lopez, B. Gardiola, M. Radovic, Elastic properties, thermal stability, and thermodynamic parameters of MoAlB, Phys. Rev. B 95 (14) (2017) 144108.
[25] G. Peipei, A. Bolon, M. Taneja, Z. Xie, N. Orlovskaya, M. Radovic, Peipei Gao, Bolon Amy, Manisha Taneja, Thermal expansion and elastic moduli of electrolyte materials for high and intermediate temperature solid oxide fuel cell, Solid State Ionics 300 (2017) 1–9.
[26] G. Pradeep, A. Muliana, M. Radovic, Pradeep Gudlur, Muliana Anastasia, Miladin Radovic, The effect of microstructural morphology on the elastic, inelastic, and degradation behaviors of aluminum–alumina composites, Mech. Res. Commun. 57 (2014) 49–56.
[27] K.M. Knowles, P.R. Howie, The directional dependence of elastic stiffness and compliance shear coefficients and shear moduli in cubic materials, J. Elast. 120 (2015) 87–108.
[28] D.H. Chung, W.R. Buessem, The elastic anisotropy of crystals, J. Appl. Phys. 38 (5) (1967).
[29] ASTM, ASTM E8 /E8M-09, Standard Test Methods for Tension Testing of Metallic Materials, ASTM International, 2009.
[30] ASTM, ASTM E21-09, Standard Test Methods for Elevated Temperature Tension Tests of Metallic Materials, ASTM International, 2009.
[31] M.M. Avedesian, H. Baker, ASM Specialty Handbook: Magnesium and Magnesium Alloys, ASM International, 1999.
[32] R. Schaller, G. Fantozzi, G. Gremaud, Grain boundary relaxation, Mechanical Spectroscopy Q-1 2001: with Application to Materials Science, Trans Tech Publications, ©2001, Switzerland ; Enfield, NH, 2001, pp. 291–340 Zuerich-Uetikon.
[33] M. Mabuchi, M. Kobata, Y. Chino, H. Iwasaki, Tensile properties of directionally solidified AZ91 Mg alloy, Mater. Trans. 44 (4) (2003) 436–439.
[34] M. Mabuchi, Y. Chino, H. Iwasaki, Tensile properties at room temperature to 823 K of Mg-4Y-3RE alloy, Mater. Trans. 43 (8) (2002) 2063–2068.
[35] H.J. Frost, Deformation-Mechanism Maps: the Plasticity and Creep of Metals and Ceramics, Pergamon Press, Oxford, 1982, p. 44.
[36] S.R. Agnew, O. Duygulu, Plastic anisotropy and the role of non-basal slip in magnesium alloy AZ31B, Int. J. Plast. 21 (2005) 1161–1193.